J Neurophysiol 123: 645–657, 2020.
First published December 18, 2019; doi:10.1152/jn.00360.2019.

RESEARCH ARTICLE | *Nervous System Pathophysiology*

The small fiber neuropathy NaV1.7 I228M mutation: impaired neurite integrity via bioenergetic and mitotoxic mechanisms, and protection by dexpramipexole

Seong-il Lee,[1,2] Janneke G. J. Hoeijmakers,[3] Catharina G. Faber,[3] Ingemar S. J. Merkies,[3,4] Giuseppe Lauria,[5,6] and Stephen G. Waxman[1,2]

[1]*Department of Neurology, Yale University School of Medicine, New Haven, Connecticut;* [2]*Center for Neuroscience and Regeneration Research, Veterans Affairs Connecticut Healthcare System, West Haven, Connecticut;* [3]*Department of Neurology, School of Mental Health and Neuroscience, Maastricht University Medical Center+, Maastricht, The Netherlands;* [4]*Department of Neurology, Curaçao Medical Center, Willemstad, Curaçao;* [5]*Neuroalgology Unit, Foundazione IRCCS Istituto Neurologico "Carlo Besta," Milan, Italy; and* [6]*Department of Biomedical and Clinical Sciences "Luigi Sacco," University of Milan, Milan, Italy*

Submitted 10 June 2019; accepted in final form 17 December 2019

Lee SI, Hoeijmakers JG, Faber CG, Merkies IS, Lauria G, Waxman SG. The small fiber neuropathy NaV1.7 I228M mutation: impaired neurite integrity via bioenergetic and mitotoxic mechanisms, and protection by dexpramipexole. *J Neurophysiol* 123: 645–657, 2020. First published December 18, 2019; doi:10.1152/jn.00360.2019.—Gain-of-function variants in voltage-gated sodium channel NaV1.7 that increase firing frequency and spontaneous firing of dorsal root ganglion (DRG) neurons have recently been identified in 5–10% of patients with idiopathic small fiber neuropathy (I-SFN). Our previous in vitro observations suggest that enhanced sodium channel activity can contribute to a decrease in length of peripheral sensory axons. We have hypothesized that sustained sodium influx due to the expression of SFN-associated sodium channel variants may trigger an energetic deficit in neurons that contributes to degeneration and loss of nerve fibers in SFN. Using an ATP FRET biosensor, we now demonstrate reduced steady-state levels of ATP and markedly faster ATP decay in response to membrane depolarization in cultured DRG neurons expressing an SFN-associated variant NaV1.7, I228M, compared with wild-type neurons. We also observed that I228M neurons show a significant reduction in mitochondrial density and size, indicating dysfunctional mitochondria and a reduced bioenergetic capacity. Finally, we report that exposure to dexpramipexole, a drug that improves mitochondrial energy metabolism, increases the neurite length of I228M-expressing neurons. Our data suggest that expression of gain-of-function variants of NaV1.7 can damage mitochondria and compromise cellular capacity for ATP production. The resulting bioenergetic crisis can consequently contribute to loss of axons in SFN. We suggest that, in addition to interventions that reduce ionic disturbance caused by mutant NaV1.7 channels, an alternative therapeutic strategy might target the bioenergetic burden and mitochondrial damage that occur in SFN associated with NaV1.7 gain-of-function mutations.

NEW & NOTEWORTHY Sodium channel NaV1.7 mutations that increase dorsal root ganglion (DRG) neuron excitability have been identified in small fiber neuropathy (SFN). We demonstrate reduced steady-state ATP levels, faster depolarization-evoked ATP decay, and reduced mitochondrial density and size in cultured DRG neurons expressing SFN-associated variant NaV1.7 I228M. Dexpramipexole, which improves mitochondrial energy metabolism, has a protective effect. Because gain-of-function NaV1.7 variants can compromise bioenergetics, therapeutic strategies that target bioenergetic burden and mitochondrial damage merit study in SFN.

bioenergetics; gain of function; mitotoxicity; NaV1.7; neuropathy

INTRODUCTION

Small fiber neuropathy (SFN) is a painful condition that typically begins to manifest symptoms such as pain and sensory loss in the extremities of the body and spreads to other regions. It is associated with depletion of intraepidermal nerve fiber (IENF) and damage to unmyelinated and thinly myelinated peripheral nerve fibers in epidermal and dermal layers of the skin. What causes the damage to these sensory nerve fibers and terminals in SFN is not well understood.

Major causes of SFN include diabetes mellitus, chemotherapy, and viral infection (Kokotis et al. 2016; Polydefkis et al. 2002; Smith et al. 2001). No apparent cause for SFN can be identified in 24% to 93% of cases in published patient series, and these cases are termed idiopathic SFN (I-SFN) (Bednarik et al. 2009; de Greef et al. 2018; Devigili et al. 2008; Lacomis 2002). Recently, Faber et al. (2012) demonstrated gain-of-function (GOF) variants in NaV1.7 in a subset of patients with idiopathic SFN. Electrophysiological assessment of these variant channels demonstrated that their altered biophysical properties render sensory neurons hyperexcitable, endowing them with a reduced threshold, increased firing frequency, and spontaneous firing of action potentials across a broad range of stimulus intensities, which can contribute to spontaneous pain (Faber et al. 2012; Han et al. 2012a, 2012b; Hoeijmakers et al. 2012b). However, little is known about the molecular or cellular bases underlying axonal injury and IENF depletion in I-SFN associated with GOF variants.

Address for reprint requests and other correspondence: S. Waxman, Dept. of Neurology, Yale University School of Medicine, 950 Campbell Ave., West Haven, CT 06516 (e-mail: stephen.waxman@yale.edu).

Downloaded from journals.physiology.org/journal/jn at Biblioteca Polo Didattico (159.149.193.179) on February 19, 2020.

Our previous in vitro observations suggest that enhanced sodium channel activity can contribute to a decrease in length of peripheral sensory axons (Persson et al. 2013b). We previously also demonstrated that the activities of normal (wild type) voltage-gated sodium channels can contribute to growth impairment and degeneration of dorsal root ganglion (DRG) neurites under metabolically challenging conditions (Persson et al. 2013a). Persistent membrane depolarization and Na^+ influx via voltage-gated sodium channels reverse the Na^+/Ca^{2+} exchanger, and the consequent ionic disturbance requires increased activity of Na^+-K^+-ATPases and Ca^{2+}-ATPases to cope with abnormal Na^+ influx and maintain ionic gradient across the membrane (Carafoli 1991; Marunaka 1988).

Mitochondria are a major ATP source in neurons and are essential for the maintenance of nerve fiber integrity (Pellerin et al. 1998; Tantama et al. 2013). Dysfunctional mitochondria have been associated with axonal degeneration in multiple neurodegenerative diseases (Persson et al. 2013a; Takeuchi et al. 2005). Mitochondrial energy metabolism is regulated by several feedback mechanisms to accommodate fluctuating energy demands that reflect dynamic neuronal activities. Increased intracellular ADP concentration ($[ADP]_i$) and Ca^{2+} influx induced by neural activity stimulate mitochondrial oxidative phosphorylation (OXPHOS) to compensate the increased ATP consumption (Lark et al. 2016; Rueda et al. 2014). Although OXPHOS constitutes an efficient mechanism to cope with abrupt increase in energy demand in neurons, its excessive activity can negatively impact mitochondrial function and bioenergetics via sustained Ca^{2+} influx and reactive oxygen species generation (Persson et al. 2016).

In this study, we tested the hypothesis that GOF variants in NaV1.7, which are associated with loss of IENFs in I-SFN, may produce a bioenergetic deficit in sensory neurons. To address this question, we employed a cell culture model and evaluated the effect of an SFN-associated variant NaV1.7, I228M, on neurite length and ATP level in DRG neurons. This particular variant was chosen for study because it previously has been characterized in detail both clinically (Faber et al. 2012) and in terms of its effect on channel and DRG neuron function (Estacion et al. 2011), and because expression of this variant within DRG neurons has a larger effect on neurite integrity in vitro than other GOF NaV1.7 mutant channels that have been studied (Persson et al. 2013b). We also examined the effect of the variant channel on mitochondria. Finally, we examined whether a drug that improves mitochondrial energy metabolism protects against the impairment of neurite length in I228M-expressing neurons.

MATERIALS AND METHODS

Plasmids. The human wild-type (WT) NaV1.7 insert (containing the adult exon 5, E5A, and Long loop1) and the NaV1.7 variant with residue substitutions I228M have been previously described (Estacion et al. 2011). Full-length inserts of clones were sequenced (Howard Hughes Medical Institute/Keck Biotechnology Center at Yale University) and analyzed using BLAST (National Library of Medicine) and Lasergene (DNAStar, Madison, WI).

ATeam1.03-nD/nA/pcDNA (ATeam), the plasmid encoding a fluorescence resonance energy transfer (FRET)-based ATP indicator, has been previously described (Imamura et al. 2009) and was purchased from Addgene (plasmid no. 51958; Addgene).

pLV-mito-DsRed, the plasmid encoding a red fluorescent protein (RFP) variant tagged with a 61-aa targeting sequence of the P1 isoform F1F0-ATP synthase (NH_2 terminal on insert) has been previously described (Kitay et al. 2013) and purchased from Addgene (plasmid no. 44386; Addgene).

Isolation and culturing of DRG neurons. All animal use procedures were approved by the Veterans Administration Connecticut Healthcare System Institutional Animal Care and Use Committee. DRG from deeply anesthetized (80 mg/kg body wt ketamine-5 mg/kg body wt xylazine) C57BL/6 mice (6–8 wk) were isolated and cultured as described previously (Estacion et al. 2011; Persson et al. 2013a). Briefly, dissected ganglia were placed in ice-cold oxygenated complete saline solution (CSS) containing (in mM) 137 NaCl, 5.3 KCl, 1 $MgCl_2$, 25 sorbitol, 3 $CaCl_2$, and 10 *N*-2-hydroxyethylpiperazine-*N*′-2-ethanesulfonic acid (HEPES), pH 7.2, and then incubated for 20 min in 37°C CSS containing collagenase A (1.5 mg/mL) and for 20 min in 37°C CSS containing collagenase D (1.5 mg/mL) and papain (30 U/mL). Ganglia were then triturated in DRG medium [DMEM/F-12 containing 100 U/mL penicillin, 0.1 mg/mL streptomycin (Invitrogen, Carlsbad, CA), 10% fetal bovine serum (Sigma-Aldrich, St. Louis, MO), 1.5 mg/mL bovine serum albumin, and 1.5 mg/mL trypsin inhibitor (Sigma)]. The cell pellet was resuspended in DRG medium.

Transfection of DRG neurons. The dissociated DRG neurons were transfected by electroporation with WT NaV1.7 channels and NaV1.7 channel variant I228M along with RFP (channel-to-RFP ratio 10:2), using Nucleofector II (program SCN6; Amaxa, Gaithersburg, MD), as previously described (Rolyan et al. 2016). WT and I228M neurons were always prepared from the same animal. After the cell suspension was isolated, it was split half and half for WT and I228M transfection so that paired cultures, prepared by the same operator on the same day from the same animal, could be compared head to head. The transfected neurons were allowed to recover for 5 min at 37°C in 0.5 mL of Ca^{2+}-free DMEM. The cell suspension was diluted with Neurobasal A medium containing 2% B-27, 1% GlutaMax, and 100 U/mL penicillin-streptomycin (Thermo Fisher Scientific), and 150 μL of the cell solution were placed on 15-mm circular poly-L-lysine/laminin-coated coverslips and incubated at 37°C in 5% CO_2 for 30 min. Standard culture medium (2 mL; Neurobasal A containing 25 mM glucose, 2% B-27, 1% GlutaMax, and 100 U/mL penicillin-streptomycin) was added and cells were maintained at 37°C in a 5% CO_2 incubator. For glucose concentration experiments (see Fig. 2), the standard culture medium (25 mM glucose) was replaced with 5.7 or 2.7 mM glucose-containing Neurobasal A.

Live-cell imaging; neurite outgrowth assay and mitochondrial morphology. Live-cell imaging for neurite measurement was performed using a Nikon Eclipse Ti microscope (Nikon USA, Melville, NY) equipped with an environmental chamber (In Vivo Scientific, St Louis, MO) to maintain the cells in a humidified atmosphere at 37°C. Tetramethylrhodamine isothiocyanate (TRITC) filter sets were used to visualize RFP fluorescence, and images were acquired using NIS-Elements (Nikon). For each coverslip, a large-field montage image consisting of 7 × 7 field-of-view images was acquired using a motorized stage and a ×10 objective.

Live-cell imaging for neuritic mitochondria was performed using the same microscope setup. For each condition, 40 images from two distinct cultures were acquired using a ×100 objective with differential interference contrast (DIC) and TRITC filter sets to create two layered images: one including mito-DsRed puncta and one including neurite morphology.

Quantification of neurite lengths. For quantification of neurite lengths, large-field images containing ~50–100 neurons (acquired as described above) were thresholded based on RFP signal using ImageJ (National Institutes of Health, Bethesda, MD; with restrictions on signal intensity, size, roundness, etc.) to create two binarized layers: one including cell bodies and one including cell bodies as well as neurites. The transfection rate for Schwann cells was very low (<0.01%) and the level of expression of RFP in these cells was low so that these cells were readily excluded by threshold setting. In addition, using roundness setting, we were also able to exclude

Downloaded from journals.physiology.org/journal/jn at Biblioteca Polo Didattico (159.149.193.179) on February 19, 2020.

Schwann cells, whose cell bodies are fusiform. With the use of particle analysis and skeletonize plugins in ImageJ (National Institutes of Health, Bethesda, MD), the total neurite length was calculated for each large-field image and divided by the number of neurons within the field. Thus a measure of the average neurite length/neuron was acquired for each large-field image. For each condition, 11–34 large-field images were analyzed from three to eight independent cultures, in each case comparing neurite length/neuron for I228M channel-transfected neurons with neurite length/neuron for WT channel-transfected neurons, cultured at the same time in parallel to ensure identical conditions. Normalized data are means ± SE, where n = number of large-field images; differences between conditions were analyzed using Student's unpaired t test, and $P < 0.05$ was considered significant.

Quantification of mitochondrial morphologies. For quantification of neuritic mitochondrial morphologies, images containing one or two neurites with mito-DsRed expression (acquired as described above) were thresholded based on DsRed signal using ImageJ. With the use of a particle analysis plugin, total number and size of DsRed puncta were measured from TRITC images. With the use of line trace and measurement tools in ImageJ, total neurite lengths were measured from DIC images. For the mitochondrial density, the total number of DsRed puncta were normalized by total length of neurites within the field. Normalized data are means ± SE; differences between conditions were analyzed using Student's unpaired t test, and $P < 0.05$ was considered significant.

ATP imaging. Somatic and intraneuritic ATP were assessed using a FRET-based ATP indicator, which increases FRET signal upon binding ATP (Imamura et al. 2009; Pathak et al. 2015). Isolated DRG neurons were transfected with ATeam1.03-nD/nA/pcDNA along with a plasmid encoding either WT or I228M mutant NaV1.7 and were cultured in poly-L-lysine/laminin-treated glass-bottom petri dishes (MatTek). At 4–7 days after plating, FRET images of the cultures were acquired in standard bath solution (SBS) containing (in mM) 140 NaCl, 3 KCl, 1 $MgCl_2$, 1 $CaCl_2$, and 10 HEPES, pH 7.3, at room temperature. Neuronal cultures were illuminated with 514-nm light to localize the neurons that were expressing the probe cotransfected with mutant I228M or WT NaV1.7 channels. Neuronal cell bodies identified from yellow fluorescent protein (YFP) signal were selected for ATP imaging. Neurons with expression of ATP indicator were illuminated with 436-nm light using a Nikon Ti-E inverted microscope equipped with a fast-switching xenon light source (Lambda DG-4; Sutter Instruments). Dual-emission ratio images were captured using a QuantEM charge-coupled device (CCD) camera (Princeton Instruments) and ×20 objective (Super Fluor; Nikon) with a DV2 beam splitter (Photometrics) and the following filter sets: 438/24, DM458, and 483/32 (CFP) or 542/27 (YFP) (Semrock, Rochester, NY). The microscope system was controlled with NIS-Elements (Nikon). Imaging data were analyzed using NIS-Elements AR (Nikon). After background correction, the YFP/CFP emission ratio was calculated by dividing yellow fluorescent protein (YFP) intensity by cyan fluorescent protein (CFP) intensity for each cell. Normalized data are means ± SE; differences between conditions were analyzed using Student's unpaired t test, and $P < 0.05$ was considered significant.

Stimulation protocol for ATP imaging. Neuronal culture dishes were microperfused at a constant flow rate using a computerized valve system (ValveLink 8.2; AutoMate Scientific). To measure $[ATP]_i$ transients in activated neuronal cell bodies and neurites, membrane depolarization was induced by perfusion with high-$[K^+]$ solution (SBS containing 50 mM KCl and 90 mM NaCl). After basal levels of [ATP] in SBS were recorded for 60 s, neurons were exposed to high-$[K^+]$ solution. During the microperfusion, neurons were illuminated every 2 s with 492-nm light using a Nikon Ti-E inverted microscope equipped with a fast-switching xenon light source (Lambda DG-4; Sutter Instruments). Time lapse images were captured using a QuantEM CCD camera (Princeton Instruments) and ×20 objective (Nikon) under the control of NIS-Elements (Nikon).

Quantification of ATP imaging. Acquired images were digitized and analyzed with NIS-Elements software (Nikon). Based on YFP signal, images were thresholded, and a binary mask was created over YFP-positive neuronal cell bodies and neurites. A binary mask overlaying each neuronal cell body was defined as a region of interest (ROI). For neurites, each 50-μm-long segment of the binary mask overlying the neurite was defined as the ROI. Fluorescence at 483-nm (CFP) and 542-nm excitation (YFP) mean pixel intensities were measured. After background correction, the ratio YFP/CFP was calculated for each image. Mean values from neuronal cell bodies and neurites are depicted in graphs. The area under the curve was calculated from time 60 s to time 180 s using Prism8 software (GraphPad). Differences between experimental groups were analyzed using Student's t test, and $P < 0.05$ was considered significant.

Statistics. Statistical analysis was performed using Prism8 software (GraphPad), and either Student's t test or the Mann–Whitney rank-sum test was used. For neurite data sets, a nested t test (Figs. 1, 5, and 7) and nested one-way ANOVA (Fig. 2) were used to accommodate cluster-related variation. Data are means ± SD. Mean difference ± SE and 95% confidence intervals were also calculated to assess the magnitude of these differences. Statistical significance was accepted at $P \leq 0.05$ for all variables.

Effect size estimates for ATP FRET. FRET in Fig. 3 is an arbitrary measurement for ATP levels. For more objective comparison of treatment effects in Fig. 3, *B* and *D*, we standardized the effect sizes, using Cohen's d effect sizes (ES) with the resulting d values reported (Cohen 1988; Lenhard and Lenhard 2016). We used an effect size calculator that considers standard deviation and sample number variation between groups as well as their nonparametric distributions (Fritz et al. 2012; Lenhard and Lenhard 2016). In this calculation, Cohen's d is computed from the equation

$$d = \frac{2r}{\sqrt{1 - r^2}},$$

where the point biserial correlation r is derived from U values from Mann–Whitney tests and sample sizes n of two groups, using Hans Wendt's formula (Wendt 1972),

$$r = \frac{1 - (2U)}{n_1 \times n_2}.$$

Availability of data and materials. The data sets that support the findings of this study have been deposited in Figshare at https://doi.org/10.6084/m9.figshare.10046105.v1.

RESULTS

I228M, an SFN-associated NaV1.7 gain of function mutant, reduces the neurite length of cultured DRG neurons. Loss of intraepidermal nerve fibers (IENFs) is a hallmark of SFN and an important diagnostic criterion of the disease. We previously reported that GOF mutations in NaV1.7 are associated with I-SFN and showed that expression of these mutations renders sensory neurons hyperexcitable. In addition, following the expression of the GOF variants, dorsal root ganglion (DRG) neurons exhibit reduced nerite lengths (Persson et al. 2013b; Rolyan et al. 2016).

To establish an in vitro model for IENF loss by SFN-associated GOF variants in NaV1.7, we transfected DRG neurons with wild-type (WT) and variant I228M NaV1.7 channels [cotransfected with red fluorescent protein (RFP) to enable the identification of transfected cells]. As demonstrated in representative 49 field-of-view montage images (Fig. 1, *A* and *C*), cultures contained numerous RFP-positive neurons, 7 days after transfection, with robust RFP signal in cell bodies as

Downloaded from journals.physiology.org/journal/jn at Biblioteca Polo Didattico (159.149.193.179) on February 19, 2020.

well as neurites. Cell diameters varied between 20 and 60 μm. Examples of neurons transfected with WT and I228M are shown at increased magnification in Fig. 1, *B* and *D*.

Mean total neurite length/neuron was quantified from large-field images for WT- and I228M-transfected neurons. There was an 20% reduction ($P < 0.0001$) in length of neurites of I228M-expressing neurons compared with those transfected with WT channels (Fig. 1*E*). We did not differentiate between large- and small-diameter DRG neurons because neurites from each neuron made multiple crossings with neurites from adjacent neurons, making it impossible to locate the cell body (or cell body diameter) from which any given neurite arose.

DRG neurons expressing I228M exhibit decreased neurite length in low glucose concentration. Neurite growth and/or the maintenance of neurite length via extension and regeneration is a high-energy demanding cellular process. Metabolically challenging conditions, especially associated with the shortage of ATP, prevent neurite extension and induce neurite degeneration (Chen et al. 2007; Estacion et al. 2015; Persson et al. 2016).

Glucose is a major substrate for ATP production, and its availability affects cellular energetics (Tanaka et al. 2014, 2015; Tantama et al. 2013). We therefore examined how low glucose availability would affect neurite growth of cultured neurons. WT channel-expressing neurons exhibited similar neurite lengths in all three glucose concentrations (25, 5.7, and 2.7mM) with a trend of modestly increased neurite length in lower concentrations (Fig. 2*A*). This result suggests that in neurons that express normal (wild type) voltage-gated sodium channels, neurite lengths are not strongly dependent on glucose availability in this model system, presumably because the channel activity and the resulting cellular activities are not a burden on neuronal bioenergetics.

In contrast to the WT cells, I228M neurons showed a trend toward markedly decreased neurite lengths at low glucose concentrations (5.7 and 2.7 mM) compared with those in the control glucose condition (25 mM; Fig. 2*B*). Average neurite length was reduced by 25% ($P = 0.015$) in 2.5 mM glucose compared with the control. Our results indicate that the presence of I228M channels imposes an energetic burden on sensory fibers, rendering them more vulnerable to damage under conditions where the glucose level is low.

DRG neurons expressing I228M exhibit a reduced steady-state level of ATP. Impaired slow inactivation of I228M is known to produce a sustained influx of sodium, which would be predicted to lead to persistent activation of Na^+-K^+-ATPase pumps (Estacion et al. 2015). The presence of I228M also produces increased spontaneous firing of DRG neurons (Estacion et al. 2011). The firing of action potentials induces synaptic vesicle cycling that imposes an additional energetic cost (Pathak et al. 2015). We therefore expected that I228M-transfected neurons would display low intracellular ATP level ($[ATP]_i$).

To address this question, we measured ATP levels in DRG neurons using a genetically encoded FRET sensor, ATeam (Imamura et al. 2009). We transfected DRG neurons with

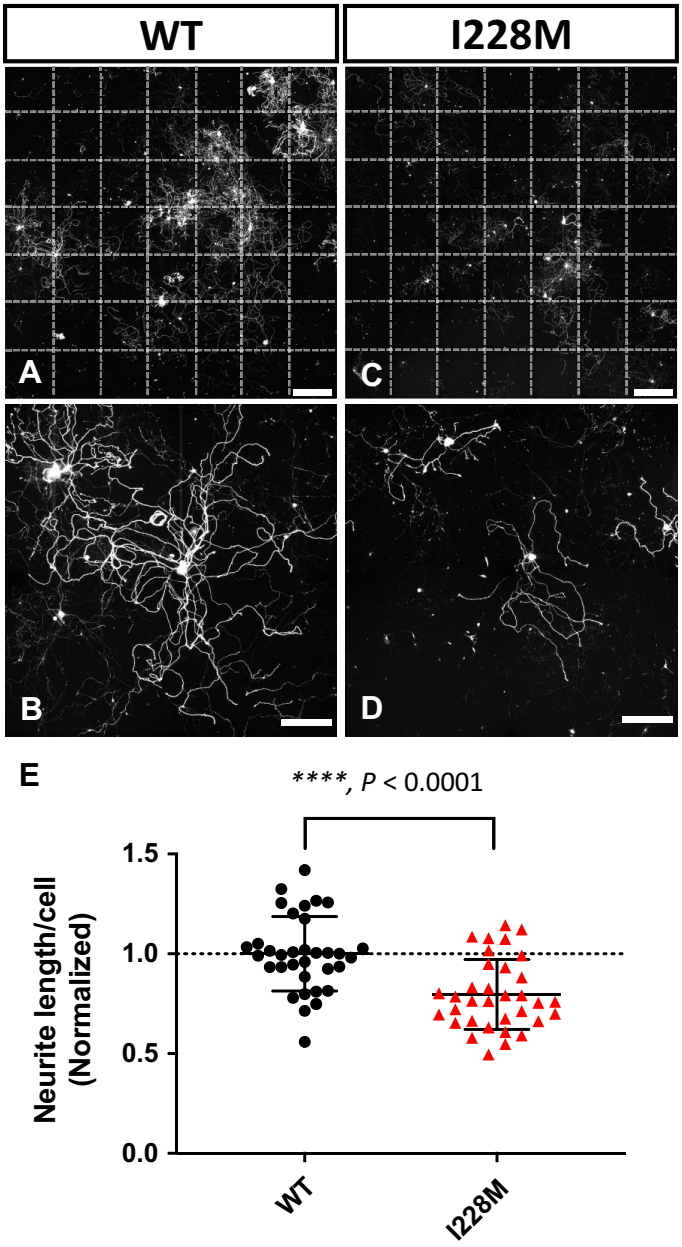

Fig. 1. Dorsal root ganglion (DRG) neurons expressing I228M, a gain-of-function mutant of NaV1.7, display reduced neurite length in vitro. Mouse DRG neurons were isolated from 6- to 8-wk-old mice, and sister cultures, prepared at the same time from the same animal by the same operator, were electroporated with the plasmid encoding wild-type (WT) NaV1.7 or the mutant channel along with red fluorescent protein (RFP). After electroporation, cells were plated on coverslips coated with laminin and cultured for 7 days. The resulting cultures were imaged and their total length per cell assessed as described in MATERIALS AND METHODS. *A*: large-field montage image of WT-expressing DRG culture, consisting of 7 × 7 field views. Dotted lines distinguish individual field of view. Scale bar, 1,000 μm. *B*: enlarged field view image of individual neurons transfected with NaV1.7 WT. *C*: large-field montage image of I228M-expressing DRG culture, consisting of 7 × 7 field views. Dotted lines distinguish individual field of view. Scale bar, 1,000 μm. *D*: enlarged field view image of individual neurons transfected with NaV1.7 I228M. *E*: quantification of total length per cell of WT and I228M neurons calculated from large-field images and the average for each condition. Each data point represents total neurite length per cell from each culture. Dotted line indicates mean value of control. Data are normalized to WT values and are means ± SD. Means of WT (n = 34 cultures from 8 animals) and I228M (34 cultures from 8 animals) are 1.000 ± 0.1870 and 0.7966 ± 0.1755, respectively. Mean difference ± SE (WT − I228M) = 0.2034 ± 0.04398; 95% confidence interval is 0.1155 to 0.2912. I228M culture displays a 20% decrease in neurite length (****$P <$ 0.0001, nested t test).

Downloaded from journals.physiology.org/journal/jn at Biblioteca Polo Didattico (159.149.193.179) on February 19, 2020.

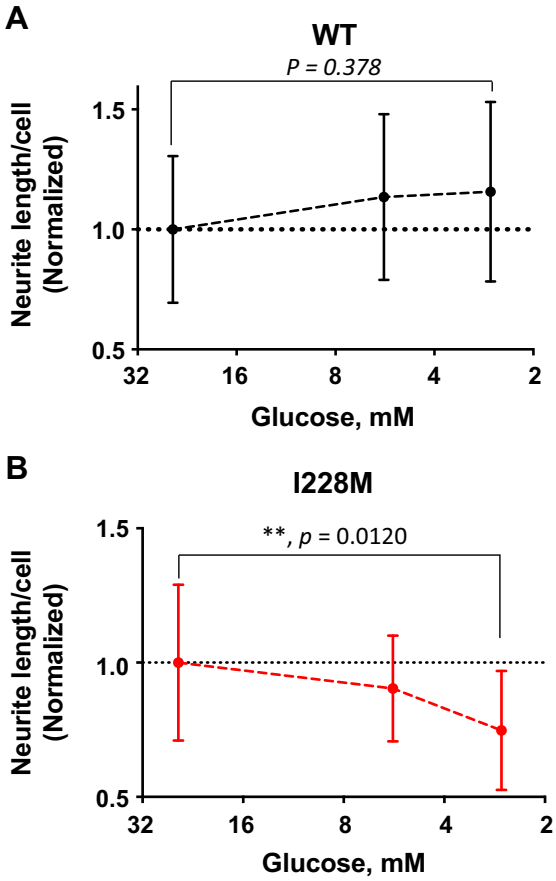

Fig. 2. Dorsal root ganglion (DRG) neurons expressing I228M display a significant reduction in neurite length at reduced glucose concentrations. Mouse DRG cultures expressing the indicated channels were prepared as described in MATERIALS AND METHODS. Cultures were then maintained in culture media containing 25, 5.7, or 2.7 mM glucose for 7 days. The resulting cultures were imaged and their neurite length assessed as described in MATERIALS AND METHODS. Data are normalized to the neurite length values of 25 mM glucose cultures and are means ± SD. Dotted line indicates mean value of control. *A*: wild-type (WT) neurons show a similar extent of neurite outgrowth in all the range of glucose concentrations (25 mM: 1 ± 0.3057, $n = 19$ cultures from 5 animals; 5.7 mM: 1.1346 ± 0.3452, $n = 19$ cultures from 5 animals; 2.7 mM: 1.1569 ± 0.3740, $n = 11$ cultures from 3 animals). *B*: I228M neurons display neurite length reduction in the low-glucose conditions compared with 25 mM glucose (25 mM: 1 ± 0.2902, $n = 20$ cultures from 5 animals; 5.7 mM: 0.9036 ± 0.1966, $n = 20$ cultures from 5 animals; 2.7 mM: 0.7471 ± 0.2218, $n = 12$ cultures from 3 animals). I228M-transfected cultures display a 25% reduction in neurite length at 2.7 mM glucose compared with cultures at 25 mM glucose (**$P = 0.0120$, nested one-way ANOVA followed by Dunnett's multiple comparisons test). Mean difference ± SE (25 mM − 2.7 mM) = 0.2529 ± 0.08847; 95% confidence interval is 0.04879 to 0.4570. In contrast to the mutant cultures, WT cultures did not show reduced neuritic growth in the low glucose concentrations (not significant; nested one-way ANOVA followed by Dunnett's multiple comparisons test).

NaV1.7 wild type (WT) or I228M along with ATeam FRET sensor and measured FRET (ratio between YFP emission and CFP emission) signals from the transfected cells 5–6 days after culturing. We compared FRET differences between WT and I228M groups.

It is not clear if the relationship of FRET values and ATP levels is linear. In recognition of this limitation, inferential statistical analysis was carried out using Cohen's *d* effect sizes (Cohen 1988), which allowed us to achieve standardized comparison of treatment effect by NaV1.7 I228M (small effect = 0.20, medium effect = 0.50, and large effect = 0.80). We calculated the effect sizes in the results of Fig. 3, using an effect size calculator that considers standard deviation and sample number variation between groups as well as their nonparametric distributions (Lenhard and Lenhard 2016).

As shown in Fig. 3, *A* and *B*, I228M neurons displayed a modest reduction in the FRET signal compared with WT neurons. Our test statistic ($P = 0.0042$) signifies this reduction in the I228M. However, given the small effect size (Cohen's $d = 0.315$, whether or not the effect size of this result is biologically meaningful remains to be determined under the conditions that might permit changes of larger magnitude in ATP level to occur.

Several feedback mechanisms might participate in the regulation of mitochondrial ATP synthesis in these neurons. A moderate ATP reduction in I228M neurons (Fig. 3*B*) might be explained as a result of increased mitochondrial metabolisms via feedback regulations (Estacion et al. 2015; Rolyan et al. 2016). We therefore treated both WT and I228M DRG cultures with 1 μM rotenone to inhibit mitochondrial function and compared their steady-state levels of ATP. Rotenone markedly reduced the FRET level in both WT and I228M cultures, indicating a significant mitochondrial contribution to the FRET signal (Fig. 3, *B* and *D*). However, in the presence of rotenone, I228M-transfected neurons showed a more robust decrease in their FRET signal compared with WT neurons. The average FRET value of WT neurons shifted from 3.738 to 3.408 (9% reduction, Cohen's $d = 0.315$), whereas the FRET signal in I228M cultures shifted from 3.542 to 3.031 (15% reduction, Cohen's $d = 0.364$; Fig. 3, *B* and *D*). This result suggests that I228M channels negatively impact neuronal bioenergetics via a reduction in $[ATP]_i$, for which mitochondria can partially compensate.

DRG neurons expressing I228M exhibit a faster decay of $[ATP]_i$ in response to membrane depolarization. DRG neurons expressing I228M channels display an increased firing frequency over a broad range of stimulus intensities even close to current threshold (Estacion et al. 2011). We therefore asked how I228M expression influences the change of $[ATP]_i$ in response to depolarization. We induced membrane depolarization in the transfected DRG neurons via application of 50 mM KCl and monitored the FRET change of the ATP sensor in real time.

As shown in Fig. 4, both WT- and I228M-transfected neurons displayed a decrease in the FRET signal of ATeam in both cell bodies and neurites in response to high-K^+ application. However, the magnitude of the FRET reduction was greater in I228M neurons than in WT neurons, suggesting that I228M neurons deplete their $[ATP]_i$ more rapidly than that of WT. More rapid reductions of the FRET signal were demonstrated in neurites than in cell bodies (Fig. 4, *B* and *D*), possibly due to the smaller diameter of neurites, which are known to express a high level of sodium channels (Black et al. 2012; Persson et al. 2010). Irrespective of the underlying biophysical mechanism, the results indicate that neurites expressing I228M channels are bioenergetically more vulnerable to energetic stress imposed by depolarization than cell bodies and that this vulnerability is markedly enhanced under the expression of I228M channels.

Pyruvate moderately increases neurite length in I228M neurons. Cellular ATP is produced in part from the activities of glycolysis and mitochondrial OXPHOS. Greater molar num-

Downloaded from journals.physiology.org/journal/jn at Biblioteca Polo Didattico (159.149.193.179) on February 19, 2020.

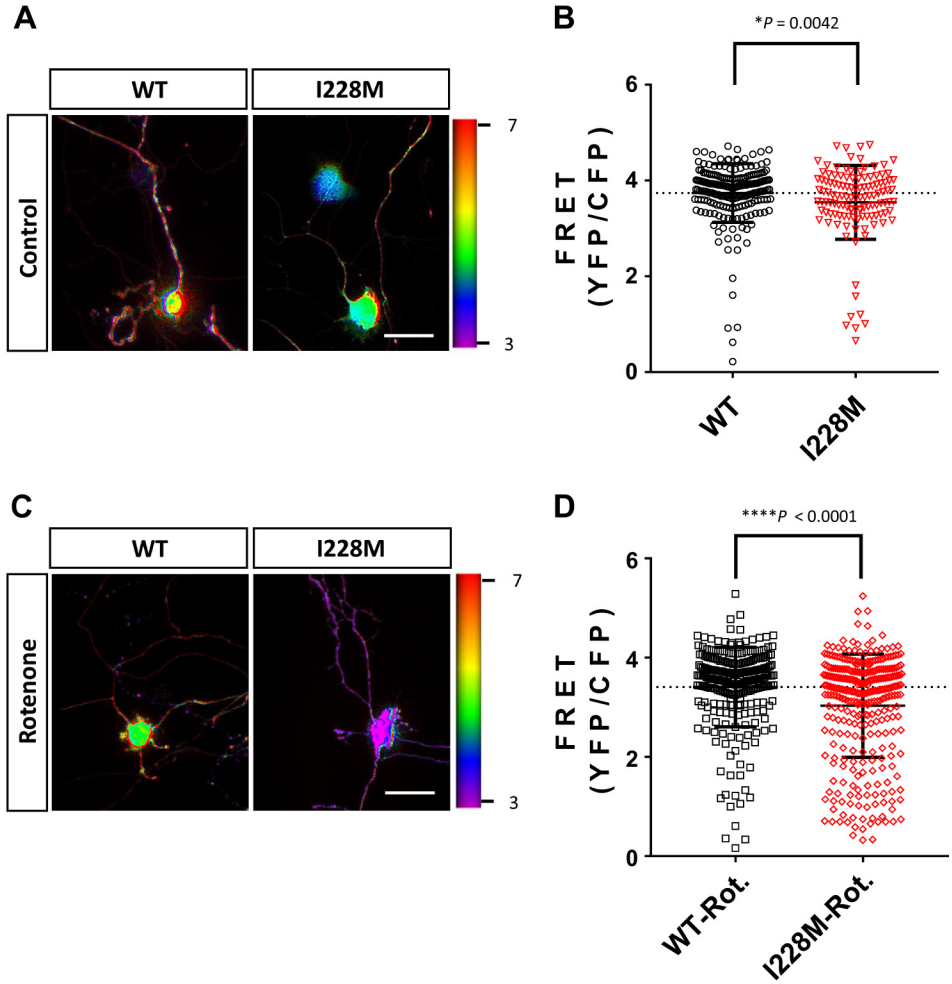

Fig. 3. Intracellular ATP levels ($[ATP]_i$) are decreased in dorsal root ganglion (DRG) neurons expressing I228M. Steady-state levels of ATP were measured from cultured DRG neurons using a fluorescence resonance energy transfer (FRET)-based ATP indicator approach. ATeam, an ATP FRET probe, was expressed in mouse DRG neurons along with the indicated channels. Seven days after culturing, FRET signals of transfected neurons were measured in the absence or presence of rotenone as described in MATERIALS AND METHODS. *A*: representative FRET images of ATeam-expressing DRG neurons. *B*: I228M-expressing neurons exhibit a reduced FRET signal compared with wild-type (WT) neurons (WT: 3.738 ± 0.612 from n = 218 cells; I228M: 3.542 ± 0.770 from n = 121 cells; $^*P = 0.0042$, Mann–Whitney test). Each data point represents a FRET value from each cell. Dotted line indicates mean value of control. *C*: representative FRET images of ATeam-expressing DRG neurons treated with rotenone. *D*: I228M-expressing neurons exhibit a markedly reduced FRET signal compared with WT neurons in the presence of rotenone (WT-Rot.: 3.408 ± 0.800 from n = 250 cells; I228M-Rot.: 3.031 ± 1.042 from n = 325 cells; $^{****}P > 0.0001$ Mann–Whitney test). Each data point represents a FRET value from each cell. Dotted line indicates mean value of control. YFP/CFP, FRET measured as ratio between yellow fluorescent protein (YFP) emission and cyan fluorescent protein (CFP) emission.

bers of ATP are synthesized from OXPHOS, utilizing pyruvate as a substrate (Fig. 5*A*). Increasing pyruvate availability has been demonstrated to facilitate mitochondrial ATP production and prevent cell and tissue damage provoked by conditions that involve bioenergetic stress (Geng et al. 2015; Izumi and Zorumski 2010; Peeling et al. 1996; So and Fuller 2003; Wang et al. 2018; Zeng et al. 2007).

We hypothesized that exogenous pyruvate might protect against the impairment of neurite outgrowth in I228M-transfected neurons. To test this hypothesis, we cultured I228M-expressing DRG neurons for 7 days in the absence and presence of pyruvate and compared the neurite lengths under these conditions. In contrast to this expectation, pyruvate treatment failed to significantly increase neurite length in I228M neurons, despite a trend of slight increase (Fig. 5*B*, *left*).

We initially reasoned that this result might reflect negative feedback regulation from glycolysis that would inactivate pyruvate dehydrogenase (Fig. 5*A*). Because high glucose concentration in the culture condition is expected to strengthen the inhibition of pyruvate dehydrogenase (PDH) through PDH kinase (PDK) phosphorylation and prevent pyruvate from being incorporated into OXPHOS, we used dichloroacetate (DCA), a PDK inhibitor, to increase pyruvate flux into mitochondrial metabolism and evaluated its effect on neurite length of I228M neurons. However, DCA treatment was also ineffective in promoting neurite length of I228M neurons (Fig. 5*B*, *right*).

I228M neurons display a marked reduction in the size and number of mitochondria. We reasoned that the failure of the previous metabolic approaches might reflect alterations of mitochondria in I228M neurons. To address this possibility, we investigated the size and density of mitochondria, which are strongly associated with the functionality and bioenergetic capacity of the organelles (Youle and van der Bliek 2012). We transfected DRG neurons with mito-DsRed, whose fluorescence is limited to mitochondria, and assessed their morphology and distribution in the transfected neurons. As shown in Fig. 6, red fluorescence was expressed as puncta along the neurites, confirming the target specificity of mito-DsRed (Kitay et al. 2013). In a comparison of WT and I228M cultures (Fig. 6), I228M-expressing neurites exhibited significantly fewer DsRed puncta than WT-expressing ones. In addition, the size of DsRed puncta in I228M-neurites was significantly diminished compared with that of WT neurites.

The extent of mitochondrial fusion and fission provides indices of the intactness of the subcellular organelle. Fragmented mitochondria, indicating increased fission, are in general associated with mitochondrial damage and reduced respiratory capacity (Rossignol et al. 2004; Westermann 2012). These results thus suggest that I228M expression leads to dysfunctional and degrading mitochondria, which is

Downloaded from journals.physiology.org/journal/jn at Biblioteca Polo Didattico (159.149.193.179) on February 19, 2020.

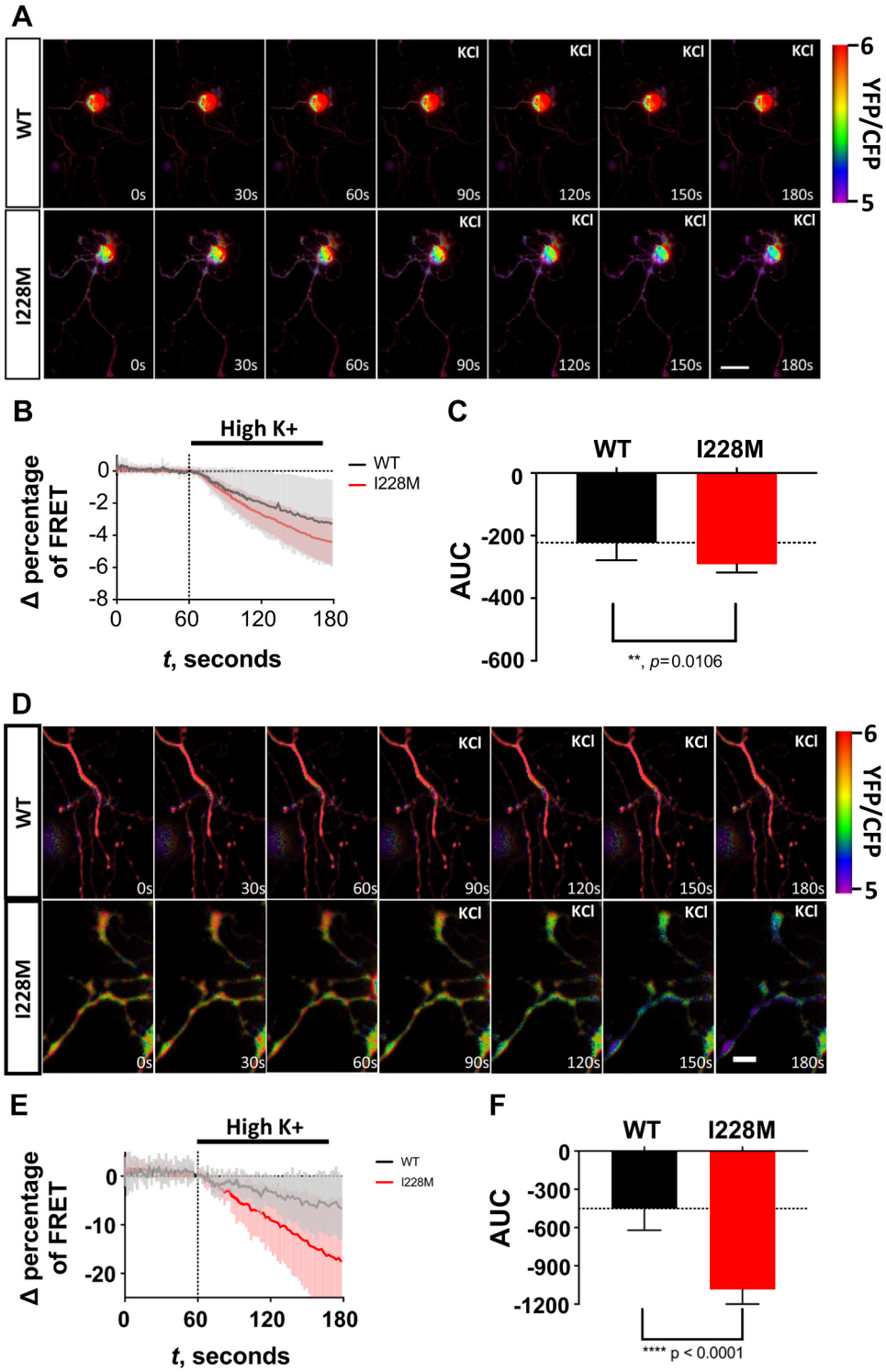

Fig. 4. Dorsal root ganglion (DRG) neurons expressing I228M display a rapid ATP reduction compared with wild-type (WT) neurons in response to membrane depolarization. ATP kinetics of DRG neurons were assessed in response to depolarization as described in MATERIALS AND METHODS. Mouse DRG neurons were transfected with ATeam along with NaV1.7 WT or I228M, and fluorescence resonance energy transfer (FRET) changes were monitored after depolarization with 50 mM KCl. *A*: representative time-lapse images of ratiometric FRET change of DRG neurons expressing the indicated channels. Scale bar, 50 μm. *B*: traces represent means of FRET change in WT neurons ($n = 8$) and I228M neurons ($n = 7$). Error bars are SD. *C*: quantification of FRET changes of DRG neurons after membrane depolarization by 50 mM K^+. Area under the curve (AUC) was calculated, and the difference between groups was analyzed (WT: -222.6 ± 56.2, $n = 8$; I228M: -291.8 ± 25.8, $n = 7$; $^{**}P < 0.0106$). Dotted line indicates mean value of control. *D*: representative time-lapse images of ratiometric FRET change of DRG neurites expressing the indicated channels. Scale bar, 10 μm. *E*: traces represent means of FRET change in WT neurites ($n = 12$) and I228M neurites ($n = 12$). Error bars are SD. F: quantification of FRET changes of DRG neurites after membrane depolarization by 50 mM K^+. Area under the curve (AUC) was calculated, and the difference between groups was analyzed (WT: -450.9 ± 169.3, $n = 12$; I228M: -1085 ± 281.2, $n = 12$; $^{****}P < 0.0001$). Dotted line indicates mean value of control.

consistent with the ineffectiveness of pyruvate and DCA treatment in neurite length enhancement. They also suggest that mitochondrial alterations are at least in part involved in the reduced cellular energy state and neurite length in the mutant cells.

Dexpramipexole increases neurite length in I228M neurons. Our results—short neurite length, impaired bioenergetics, and mitochondrial alterations in I228M neurons—predict that agents that protect or restore mitochondrial energy production might protect against the impairment of neurite length by GOF variants in NaV1.7. An electrochemical gradient of protons is created by cellular respiratory activities of mitochondria. The ionic gradient across the inner mitochondrial membrane is used to drive ATP synthesis. Maintaining the gradient is, therefore, critical to ensure sufficient ATP production via mitochondrial OXPHOS.

The mitochondrial permeability transition pore (mPTP) is known to regulate the ionic gradient in mitochondrial matrix.

Downloaded from journals.physiology.org/journal/jn at Biblioteca Polo Didattico (159.149.193.179) on February 19, 2020.

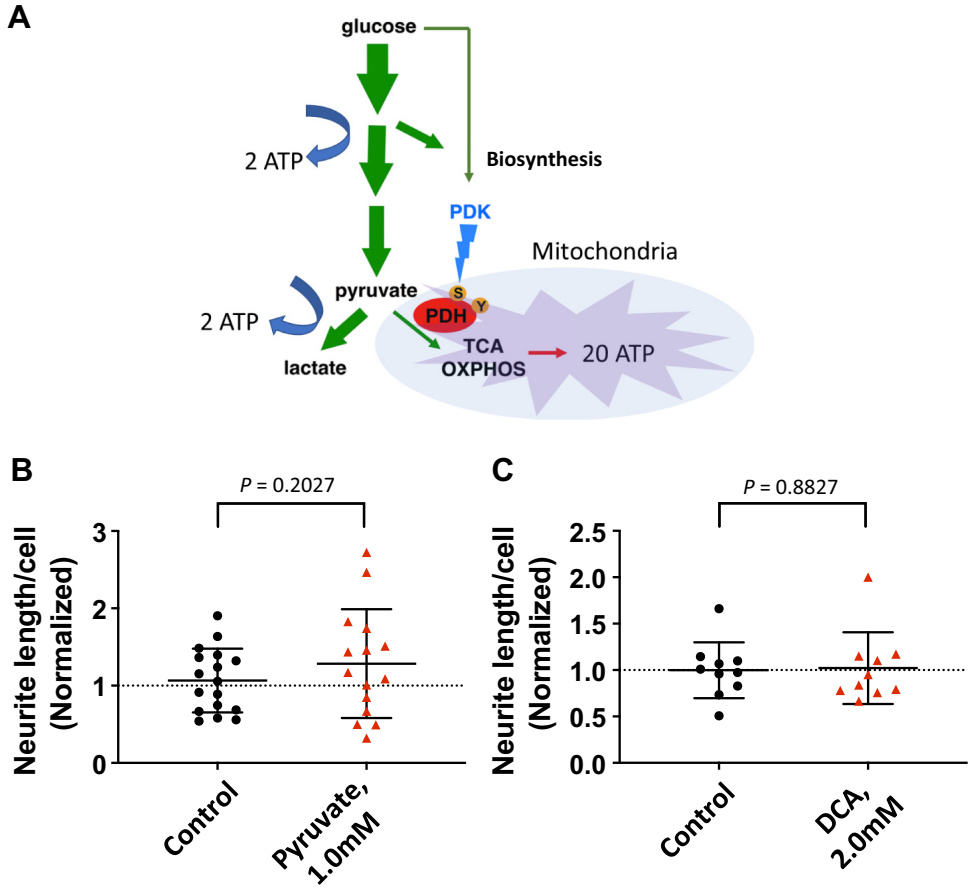

Fig. 5. Increasing pyruvate availability fails to increase the neurite length of I228M neurons. I228M neurons were treated as indicated, to increase pyruvate availability for mitochondria and assess the effects of those treatments on the neuritic growth. Mouse dorsal root ganglion neurons were isolated from 6- to 8-wk-old mice and electroporated with the plasmid encoding wild-type (WT) NaV1.7 or the mutant channel along with red fluorescent protein (RFP). After electroporation, cells were plated on coverslips coated with laminin and cultured for 7 days in the indicated treatments. *A*: carbohydrate energy metabolism and its feedback regulation. Using pyruvate, mitochondria produce more ATP through the tricarboxylic acid (TCA) cycle and oxidative phosphorylation (OXPHOS) than through glycolysis and lactate fermentation. Glucose negatively regulates mitochondrial TCA and OXPHOS via pyruvate dehydrogenase kinase (PDK). *B*: effect of pyruvate supplementation on neurite length. Each data point represents total neurite length per cell from each culture. Dotted line indicates mean value of control. Data are normalized to the value of I228M control (without pyruvate) and are means ± SD (I228M control: 1.067 ± 0.413, $n = 17$ cultures from 6 animals; I228M pyruvate, 1.0 mM: 1.284 ± 0.704, $n = 15$ cultures from 6 animals). Difference between means is not significant ($P = 0.2027$, nested t test): mean ± SE (control − pyruvate) = −0.4249 ± 0.3117; 95% confidence interval is −1.120 to 0.2696. *C*: effect of dichloroacetate (DCA) treatment on neurite length. Each data point represents total neurite length per cell from each culture. Dotted line indicates mean value of control. Data are normalized to the value of I228M-Control (without DCA treatment) and are means ± SD (I228M control: 0.9981 ± 0.301, $n = 12$ cultures from 3 animals; I228M DCA, 2.0 mM: 1.021 ± 0.387, $n = 10$ cultures from 3 animals). Difference between means is not significant ($P = 0.8827$, nested t test): mean ± SE (control − DCA) = −0.02322 ± 0.1551; 95% confidence interval is −0.3490 to 0.3026.

Despite its role in the regulation of mitochondrial Ca^{2+} level and metabolism, pathological conditions related to energetic stress and Ca^{2+} overload can cause prolonged opening of mPTP, and in turn induce mitochondrial dysfunction.

Dexpramipexole (DEX) blocks mPTP, enhances mitochondrial membrane potential, and improves mitochondrial energy metabolism in models of neurodegeneration (Alavian et al. 2012, 2015). To determine whether DEX protects against reduced neurite length of I228M neurons, we treated the neurons with this drug at a concentration previously reported to increase ATP levels in neuronal cultures (Alavian et al. 2012). As shown in Fig. 7*E*, treated neurons displayed a significant increase in neurite length compared with the untreated group in parallel cultures. Mean total length per neuron was increased by 25% in DEX-treated I228M neurons. We also assessed the effect of DEX on WT neurons and found that 2 μM DEX did not alter neurite length of WT-transfected neurons (Fig. 7*F*).

Those results indicate that mitochondrial mechanisms are indeed involved in the neuritic impairment of I228M neurons. They also suggest that a therapeutic strategy might target mitochondrial dysfunction to prevent IENF loss that occurs in DRG neurons carrying GOF mutations in NaV1.7.

DISCUSSION

Gain-of-function mutations in NaV1.7 are related to loss of intraepidermal nerve fibers in I-SFN and reduce neurite lengths in cultured DRG neurons. The epidermis where IENFs reside is a dynamic terrain. The tissue continuously remodels itself. Because new keratinocytes arise at the base of the tissue and then migrate upward and flatten preexisting keratinocytes, there is an ongoing change of intercellular space and extracellular matrix, which mandates IENFs to navigate through and adjust their ramification patterns while

Downloaded from journals.physiology.org/journal/jn at Biblioteca Polo Didattico (159.149.193.179) on February 19, 2020.

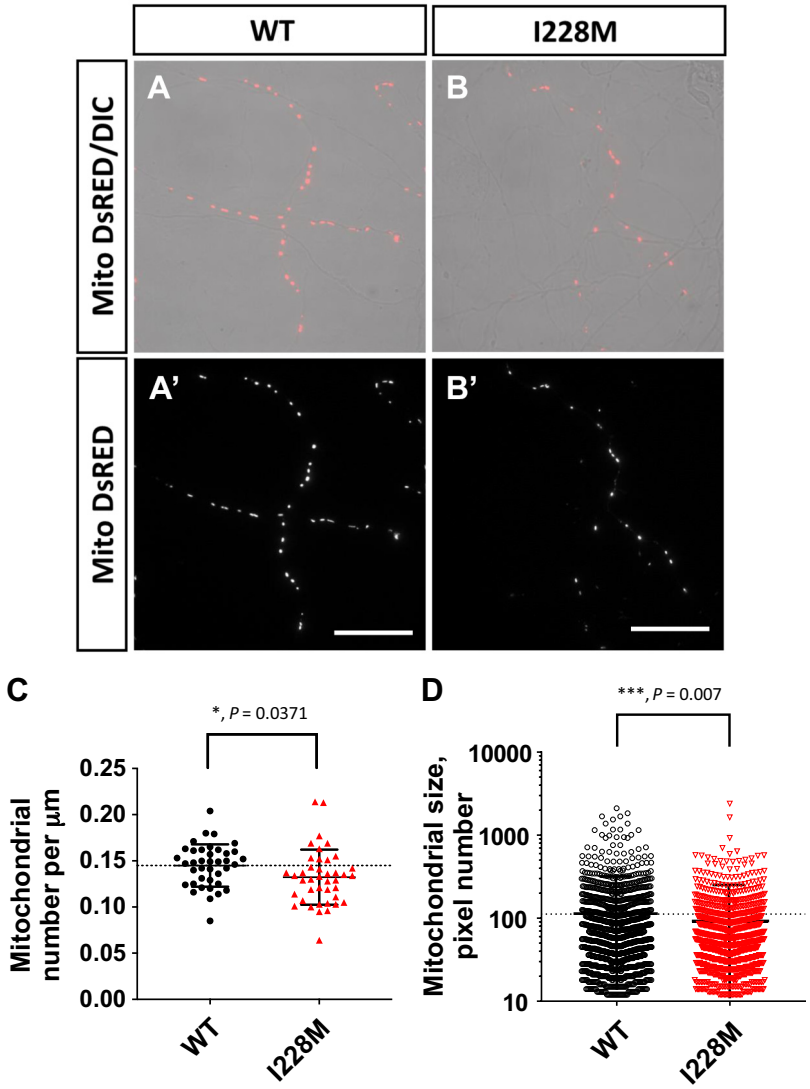

Fig. 6. I228M-expressing neurons exhibit alterations in mitochondrial distribution and morphology. Mitochondria were genetically labeled by transfecting mito-DsRed into mouse dorsal root ganglion (DRG) neurons expressing the indicated human NaV1.7 plasmids. Mitochondria with red fluorescence were imaged and counted in transfected neurites, as described in MATERIALS AND METHODS. *A* and *A′*: representative images of neuritic mitochondria of DRG neurons expressing wild type (WT), with and without differential interference contrast (DIC), respectively. Scale bar, 50 μm. *B* and *B′*: representative images of neuritic mitochondria of DRG neurons expressing I228M, with and without DIC, respectively. Scale bar, 50 μm. *C*: mitochondrial density of WT- and I228M-expressing neurites. Dotted line indicates mean value of control. Each data point represents an individual neurite. Data are normalized to neurite length and are mean ± SD mitochondrial numbers per μm (WT: 0.1449 ± 0.0229, n = 39 neurites; I228M: 0.1323 ± 0.0046610298, n = 41 neurites; *P = 0.0371, unpaired t test). Mean difference ± SE (WT − I228M) = 0.01266 ± 0.005967; 95% confidence interval is −0.02453 to −0.00078. *D*: mitochondrial size of WT- and I228M-expressing neurites. Dotted line indicates mean value of control. Each data point represents an individual mitochondria. Data are mean ± SD pixel numbers (WT: 112 ± 171.59, n = 1453 mitochondria; I228M: 90.47 ± 130.01, n = 1014 mitochondria; ***P = 0.007, Mann–Whitney test). I228M neurons display a modest but significant reduction in mitochondrial density and size in neurites compared with WT neurons.

maintaining their skin innervation. IENFs achieve this goal by a dynamic process that involves repeated regeneration and degeneration (Cheng et al. 2010; Gibbons et al. 2010; Verzé et al. 1999).

Previous skin biopsy studies have revealed that the density of nerve fibers innervating the epidermis is reduced, and some nerve fiber terminals display degenerating or retracting morphologies in the epidermis of SFN patients harboring GOF mutations in NaV1.7. Those observations suggest that the sensory nerve fibers in SFN are "dying back" (Chai et al. 2005; Hoeijmakers et al. 2012a; Lauria et al. 2011).

The neurite outgrowth assay provides a simple in vitro method for assessment of potential effects of genetic and exogenous factors on the integrity of the axons of DRG neurons. (Filous and Silver 2016). In the present study, we chose the I228M mutation of NaV1.7 because it has been characterized in detail both clinically (Faber et al. 2012) and in terms of its effect on channel and DRG neuron function (Estacion et al. 2011) and because expression of this variant within DRG neurons has a larger effect on neurite integrity in vitro than other gain-of-function NaV1.7 mutant channels that have been studied (Persson et al. 2013b). Using this in vitro assay, DRG neurons transfected with I228M showed a reduced neurite length compared with WT channels (Fig. 1).

Gain-of-function mutations in NaV1.7 produce a bioenergetic deficit. Despite the statistical significance of our results in Fig. 3, their small effect sizes approximately equate to a 58.4–61.1% probability of superiority, suggesting that the effect of I228M in this condition might be minimal at best (calculated from https://rpsychologist.com/d3/cohend/). Whether or not a 0.3–0.4 standard deviation difference between groups is biologically relevant remains to be determined through further investigation. In SFN patients, neurodegeneration occurs in length-dependent and age-dependent manners (Hoeijmakers et al. 2012a). Given this clinical feature of SFN, culturing for longer periods of time, under conditions that permit growth of longer axons and cumulative ATP reduction or mitotoxic effect, might permit changes of larger magnitude in ATP level to occur.

I228M-expressing neurons demonstrated reduced levels of $[ATP]_i$ in the basal state and increased ATP consumption rates in response to depolarization (Figs. 3 and 4). These results suggest that decreased bioenergetic stores contribute to the pathophysiology of SFN related to GOF variants of NaV1.7.

Downloaded from journals.physiology.org/journal/jn at Biblioteca Polo Didattico (159.149.193.179) on February 19, 2020.

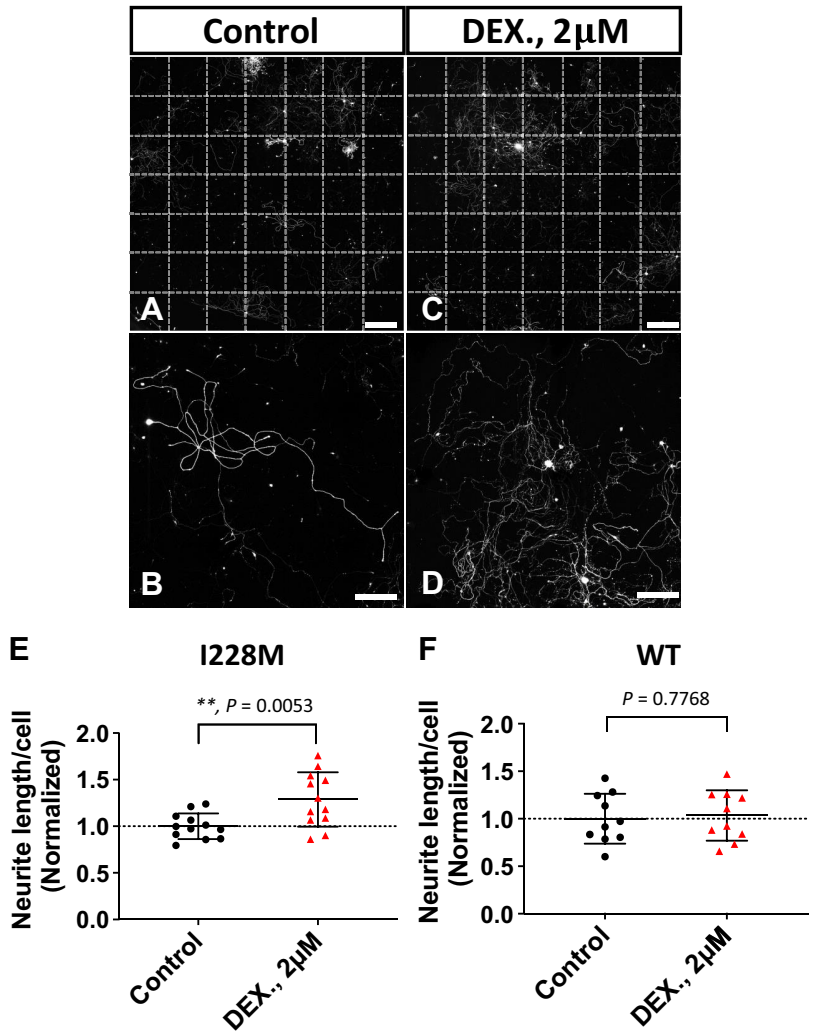

Fig. 7. Dexpramipexole (DEX) promotes neurite growth of I228M-expressing neurons. I228M neurons were treated with 2 μM DEX for 7 days, and neurite length was compared with that of untreated neurons (control). *A*: representative montaged image of I228M-expressing dorsal root ganglion (DRG) culture. *B*: field view image of the montaged image shown in *A*. *C*: representative montaged image of I228M-expressing DRG culture on a coverslip. *D*: field view image of the montaged image shown in *C*. *E*: quantification of total length per cell for I228M control and I228M DEX treatment groups. Dotted line indicates mean value of control. Each data point represents total neurite length per cell from each culture. Data are normalized to neurite control value and are means ± SD (I228M control: 1 ± 0.0974, n = 12 cultures from 3 animals; I228M DEX, 2 μM: 1.287 ± 0.08403, n = 12 cultures from 3 animals). Mean difference ± SE (DEX − control) = 0.2875 ± 0.09296; 95% confidence interval is −0.009469 to 0.4803. DEX-treated I228M cultures display a 29% increase in neurite length (**P = 0.0053, nested t test). *F*: quantification of total length per cell of wild-type (WT) control and WT DEX treatment groups. Dotted line indicates mean value of control. Each data point represents total neurite length per cell from each culture. Data are normalized to neurite control value and are means ± SD (WT control: 1 ± 0.0828 from n = 10 cultures from 3 animals; WT DEX, 2 μM: 1.034 ± 0.0839, n = 10 cultures from 3 animals). Mean difference ± SE (DEX − control) = −0.03392 ± 0.1179; 95% confidence interval is −0.2816 to 0.2138. DEX-treated WT cultures did not display any significant change in neurite length (P = 0.7768, nested t test).

Those mutations alter the gating properties of the channels so that their pores open more frequently and/or with longer duration (Estacion et al. 2011; Hoeijmakers et al. 2012b). Those alterations expectedly increase Na^+ influx and, via reverse operation of Na^+/Ca^{2+} exchanger, alter $[Ca^{2+}]_i$ dynamics in neurons as demonstrated by the example of G856D mutation (Estacion et al. 2015). To reverse the resulting ionic imbalance, the excessive Na^+ and Ca^{2+} are necessarily pumped out, which requires increasing activities of Na^+-K^+-ATPase and Ca^{2+}-ATPase (Ames et al. 1992; Palmgren and Nissen 2011; Sokoloff 1999). The increased activities of these pumps can impose an energetic burden to neurons. In addition to that ionic disturbance, the variant channels render neurons hyperexcitable with higher firing frequency and increased spontaneous firing of action potentials that can confer an additional energetic burden (Estacion et al. 2011; Han et al. 2012a, 2012b; Hoeijmakers et al. 2012a).

Cellular energy state influences neurite length. Multiple studies have suggested a link between bioenergetic state and the maintenance of axonal integrity (Chowdhury et al. 2014; Estacion et al. 2015; Persson et al. 2013a). Numerous cellular events take part in axon extension and maintenance, including actin-microtubule reorganization, vesicle trafficking, and protein synthesis, and some of them are energetically demanding. It is thus not surprising that impaired bioenergetic states have been shown to result in axonal injury, growth inhibition, and degeneration in vitro (Gibbons et al. 2010; Kitayama et al. 2008; Natera-Naranjo et al. 2012; Persson et al. 2013a; Press and Milbrandt 2008). The continuous remodeling that is required for IENFs in vivo to maintain skin innervation as they accommodate to the addition of new epidermal cells and their transit to the skin surface may add to the energetic demand.

Our results suggest that a bioenergetic deficit contributes to the mechanism by which GOF variants in NaV1.7 cause IENF loss. First, under the expression of I228M mutant channels, DRG neurons displayed reduced steady-state levels of $[ATP]_i$ and rapid ATP consumption rates upon membrane depolarization. This result indicates that the mutant channels impose bioenergetic stress on sensory neurons and their nerve fibers. Second, neurite lengths in I228M neurons were markedly sensitive to glucose availability, whereas this effect was not observed in WT cells. This result suggests that the energetic burden by GOF variants in NaV1.7 renders nerve fibers vulnerable to metabolic conditions that are benign to WT axons. Given that the low glucose concentrations that we used fall within physiological ranges (Güemes et al. 2016), we suggest that the GOF variant channels trigger axonal damage, at least in part, via a bioenergetic mechanism in I-SFN.

Downloaded from journals.physiology.org/journal/jn at Biblioteca Polo Didattico (159.149.193.179) on February 19, 2020.

Mitotoxicity and protection in peripheral sensory neuropathies. The alterations of mitochondria in I228M neurons (Fig. 6) indicate that mitochondrial mechanisms also contribute to impaired bioenergetics and IENF damage in I-SFN related to NaV1.7 mutations. Dysfunction and/or loss of mitochondria has been recently suggested as a converging pathogenic mechanism in multiple types of peripheral neuropathy (Bennett et al. 2014; Casanova-Molla et al. 2012; Lehmann et al. 2011; Persson et al. 2016). DEX has been shown to have a protective effect in several models of neurodegeneration (Alavian et al. 2012, 2015). The beneficial effect of DEX in our model system (Fig. 7) suggests the possibility that, at least in the short term, a degree of therapeutic protection of IENF may be achievable.

Bioenergetic stress and pain. Bioenergetic stress impairs the performance of Na^+-K^+-ATPase-dependent pump. This impairment contributes to a depolarizing shift in resting membrane potential, which can render neurons hyperexcitable before development of neuropathy (Nasu et al. 2014). Ischemic conditions are also known to result in bioenergetic deficits and increase membrane depolarization and axonal excitability (Han et al. 2008; Kiernan and Bostock 2000). Those results are consistent with our hypothesis and observations: GOF variants in NaV1.7 evoke bioenergetic stress, resulting in the impairment of the ATPases pumps and a disturbance of ionic gradient. We suggest that the ionic disturbance evoked by the variant channels and the consequent energetic burden may mutually amplify each other. The resulting positive feedback loop may, in the long term, aggravate spontaneous impulse generation and pain in SFN. For instance, increased ionic perturbation would decrease cellular energy. This energy crisis would consequently impair the function of the ATPase-dependent ion pumps. As a result, the residual ionic imbalance would be expected to persistently activate ATPases, further depriving cellular ATP. Through this cycling between ionic imbalance and bioenergetic stress, neurons would be increasingly depolarized and deprived of cellular energy. If affected neurons are nociceptors, this would contribute to an increased spontaneous pain. If such a cycling persists, the consequent severe bioenergetic crisis would lead to neurodegeneration of IENF.

Multiple GOF mutations of NaV1.7 have been linked to small fiber neuropathy (Faber et al. 2012; Han et al. 2012a, 2012b). In previous studies, a subset of DRG neurons expressing the SFN G856D mutation demonstrated time-dependent neurite degeneration as well as neurite fragmentation under metabolically challenging conditions (Estacion et al. 2015; Rolyan et al. 2016). However, the G856D mutation produces a complex phenotype in which impaired distal limb development accompanies SFN (Hoeijmakers et al. 2012b). We speculate that many gain-of-function NaV1.7 mutations impose energetic stress on DRG neurons. Additional studies on other NaV1.7 mutant channels will be needed to confirm this proposal. Additional studies will be needed to determine whether bioenergetic or mitotoxic mechanisms contribute to the association that has been reported (Blesneac et al. 2018) between NaV1.7 mutations and painful diabetic neuropathy.

Conclusion. SFN is a progressive disorder and is often diagnosed when there is degeneration of nerve fibers. Our result suggests that in addition to interventions that selectively reduce ionic imbalances caused by mutant NaV1.7 channels, an alternative therapeutic strategy might target the bioenergetic burden and mitochondrial dysfunction that occur in SFN associated with NaV1.7 gain-of-function mutations. Future studies are needed to assess this approach with multiple SFN-associated sodium channel mutations and should aim at testing this mechanism in vivo, via the assessment of IENF and behavioral changes after interventions that protect bioenergetic mechanisms.

ACKNOWLEDGMENTS

We thank Peng Zhao and Lawrence Macala for superb technical assistance and Monique M. Gerrits and Daria Sizova for helpful suggestions.

GRANTS

This work was supported by the Rehabilitation Research Service and Biomaedical Laboratory Research Service, U.S. Department of Veterans Affairs, and by Prinses Beatrix Spierfonds Grant 721841 (to S. G. Waxman).

DISCLOSURES

C.G. Faber reports grants from European Union's Horizon 2020 research and innovation program Marie Sklodowska-Curie grant for PAIN-Net, Molecule-to-man pain network (grant no. 721841), grants from Prinses Beatrix Spierfonds, grants from Grifols and Lamepro for a trial on IVIg in small fiber neuropathy, and others from Steering committees/advisory board for studies in small fiber neuropathy of Biogen/Convergence and Vertex, outside the submitted work.

I.S.J. Merkies reports participation in steering committees of the Talecris ICE Study, CSL Behring, LFB, Novartis, Octapharma, Biotest and UCB, grants from Grifols and Lamepro for a trial on IVIg in small fiber neuropathy, outside the submitted work.

J.G.J. Hoeijmakers reports a grant from Prinses Beatrix Spierfonds, outside the submitted work. S. G. Waxman reports serving as an advisor or consultant to Amgen, Biogen, GlaxoSmithKline, Chromocell, and SiteOne Therapeutics.

None of the other authors has any conflicts of interest, financial or otherwise, to disclose.

AUTHOR CONTRIBUTIONS

S.I.L. and S.G.W. conceived and designed research; S.I.L. performed experiments; S.I.L. analyzed data; S.I.L. and S.G.W. interpreted results of experiments; S.I.L. prepared figures; S.I.L. and S.G.W. drafted manuscript; S.I.L., J.G.J.H., C.G.F., I.S.J.M., G.L., and S.G.W. edited and revised manuscript; S.I.L., J.G.J.H., C.G.F., I.S.J.M., G.L., and S.G.W. approved final version of manuscript.

REFERENCES

Alavian KN, Dworetzky SI, Bonanni L, Zhang P, Sacchetti S, Li H, Signore AP, Smith PJ, Gribkoff VK, Jonas EA. The mitochondrial complex V-associated large-conductance inner membrane current is regulated by cyclosporine and dexpramipexole. *Mol Pharmacol* 87: 1–8, 2015. doi:10.1124/mol.114.095661.

Alavian KN, Dworetzky SI, Bonanni L, Zhang P, Sacchetti S, Mariggio MA, Onofrj M, Thomas A, Li H, Mangold JE, Signore AP, Demarco U, Demady DR, Nabili P, Lazrove E, Smith PJ, Gribkoff VK, Jonas EA. Effects of dexpramipexole on brain mitochondrial conductances and cellular bioenergetic efficiency. *Brain Res* 1446: 1–11, 2012. doi:10.1016/j.brainres.2012.01.046.

Ames A 3rd, Li YY, Heher EC, Kimble CR. Energy metabolism of rabbit retina as related to function: high cost of Na^+ transport. *J Neurosci* 12: 840–853, 1992. doi:10.1523/JNEUROSCI.12-03-00840.1992.

Bednarik J, Vlckova-Moravcova E, Bursova S, Belobradkova J, Dusek L, Sommer C. Etiology of small-fiber neuropathy. *J Peripher Nerv Syst* 14: 177–183, 2009. doi:10.1111/j.1529-8027.2009.00229.x.

Bennett GJ, Doyle T, Salvemini D. Mitotoxicity in distal symmetrical sensory peripheral neuropathies. *Nat Rev Neurol* 10: 326–336, 2014. [Erratum in *Nat Rev Neurol* 10: 428, 2014.] doi:10.1038/nrneurol.2014.77.

Black JA, Frézel N, Dib-Hajj SD, Waxman SG. Expression of Nav1.7 in DRG neurons extends from peripheral terminals in the skin to central preterminal branches and terminals in the dorsal horn. *Mol Pain* 8: 82, 2012. doi:10.1186/1744-8069-8-82.

Downloaded from journals.physiology.org/journal/jn at Biblioteca Polo Didattico (159.149.193.179) on February 19, 2020.

Blesneac I, Themistocleous AC, Fratter C, Conrad LJ, Ramirez JD, Cox JJ, Tesfaye S, Shillo PR, Rice AS, Tucker SJ, Bennett DL. Rare NaV1.7 variants associated with painful diabetic peripheral neuropathy. *Pain* 159: 469–480, 2018. doi:10.1097/j.pain.0000000000001116.

Carafoli E. Calcium pump of the plasma membrane. *Physiol Rev* 71: 129–153, 1991. doi:10.1152/physrev.1991.71.1.129.

Casanova-Molla J, Morales M, Garrabou G, Solà-Valls N, Soriano A, Calvo M, Grau JM, Valls-Solé J. Mitochondrial loss indicates early axonal damage in small fiber neuropathies. *J Peripher Nerv Syst* 17: 147–157, 2012. doi:10.1111/j.1529-8027.2012.00396.x.

Chai J, Herrmann DN, Stanton M, Barbano RL, Logigian EL. Painful small-fiber neuropathy in Sjogren syndrome. *Neurology* 65: 925–927, 2005. doi:10.1212/01.wnl.0000176034.38198.f9.

Chen W, Mi R, Haughey N, Oz M, Höke A. Immortalization and characterization of a nociceptive dorsal root ganglion sensory neuronal line. *J Peripher Nerv Syst* 12: 121–130, 2007. doi:10.1111/j.1529-8027.2007.00131.x.

Cheng C, Guo GF, Martinez JA, Singh V, Zochodne DW. Dynamic plasticity of axons within a cutaneous milieu. *J Neurosci* 30: 14735–14744, 2010. doi:10.1523/JNEUROSCI.2919-10.2010.

Chowdhury SR, Saleh A, Akude E, Smith DR, Morrow D, Tessler L, Calcutt NA, Fernyhough P. Ciliary neurotrophic factor reverses aberrant mitochondrial bioenergetics through the JAK/STAT pathway in cultured sensory neurons derived from streptozotocin-induced diabetic rodents. *Cell Mol Neurobiol* 34: 643–649, 2014. doi:10.1007/s10571-014-0054-9.

Cohen J. *Statistical Power Analysis for the Behavioral Sciences* (2nd ed.). Hillsdale, NJ: Erlbaum, 1988.

de Greef BT, Hoeijmakers JG, Gorissen-Brouwers CM, Geerts M, Faber CG, Merkies IS. Associated conditions in small fiber neuropathy — a large cohort study and review of the literature. *Eur J Neurol* 25: 348–355, 2018. doi:10.1111/ene.13508.

Devigili G, Tugnoli V, Penza P, Camozzi F, Lombardi R, Melli G, Broglio L, Granieri E, Lauria G. The diagnostic criteria for small fibre neuropathy: from symptoms to neuropathology. *Brain* 131: 1912–1925, 2008. doi:10.1093/brain/awn093.

Estacion M, Han C, Choi JS, Hoeijmakers JG, Lauria G, Drenth JP, Gerrits MM, Dib-Hajj SD, Faber CG, Merkies IS, Waxman SG. Intra- and interfamily phenotypic diversity in pain syndromes associated with a gain-of-function variant of NaV1.7. *Mol Pain* 7: 92, 2011. doi:10.1186/1744-8069-7-92.

Estacion M, Vohra BP, Liu S, Hoeijmakers J, Faber CG, Merkies IS, Lauria G, Black JA, Waxman SG. Ca^{2+} toxicity due to reverse Na^{+}/Ca^{2+} exchange contributes to degeneration of neurites of DRG neurons induced by a neuropathy-associated Nav1.7 mutation. *J Neurophysiol* 114: 1554–1564, 2015. doi:10.1152/jn.00195.2015.

Faber CG, Hoeijmakers JG, Ahn HS, Cheng X, Han C, Choi JS, Estacion M, Lauria G, Vanhoutte EK, Gerrits MM, Dib-Hajj S, Drenth JP, Waxman SG, Merkies IS. Gain of function $Na_V1.7$ mutations in idiopathic small fiber neuropathy. *Ann Neurol* 71: 26–39, 2012. doi:10.1002/ana.22485.

Filous AR, Silver J. Neurite outgrowth assay. *Bio Protoc* 6: 6, 2016. doi:10.21769/BioProtoc.1694.

Fritz CO, Morris PE, Richler JJ. Effect size estimates: current use, calculations, and interpretation. *J Exp Psychol Gen* 141: 2–18, 2012. doi:10.1037/a0024338.

Geng X, Elmadhoun O, Peng C, Ji X, Hafeez A, Liu Z, Du H, Rafols JA, Ding Y. Ethanol and normobaric oxygen: novel approach in modulating pyruvate dehydrogenase complex after severe transient and permanent ischemic stroke. *Stroke* 46: 492–499, 2015. doi:10.1161/STROKEAHA.114.006994.

Gibbons CH, Wang N, Freeman R. Capsaicin induces degeneration of cutaneous autonomic nerve fibers. *Ann Neurol* 68: 888–898, 2010. doi:10.1002/ana.22126.

Güemes M, Rahman SA, Hussain K. What is a normal blood glucose? *Arch Dis Child* 101: 569–574, 2016. doi:10.1136/archdischild-2015-308336.

Han C, Hoeijmakers JG, Ahn HS, Zhao P, Shah P, Lauria G, Gerrits MM, te Morsche RH, Dib-Hajj SD, Drenth JP, Faber CG, Merkies IS, Waxman SG. Nav1.7-related small fiber neuropathy: impaired slow-inactivation and DRG neuron hyperexcitability. *Neurology* 78: 1635–1643, 2012a. doi:10.1212/WNL.0b013e3182574f12.

Han C, Hoeijmakers JG, Liu S, Gerrits MM, te Morsche RH, Lauria G, Dib-Hajj SD, Drenth JP, Faber CG, Merkies IS, Waxman SG. Functional profiles of SCN9A variants in dorsal root ganglion neurons and superior cervical ganglion neurons correlate with autonomic symptoms in small fibre neuropathy. *Brain* 135: 2613–2628, 2012b. doi:10.1093/brain/aws187.

Han SE, Boland RA, Krishnan AV, Vucic S, Lin CS, Kiernan MC. Changes in human sensory axonal excitability induced by an ischaemic insult. *Clin Neurophysiol* 119: 2054–2063, 2008. doi:10.1016/j.clinph.2008.04.295.

Hoeijmakers JG, Faber CG, Lauria G, Merkies IS, Waxman SG. Small-fibre neuropathies—advances in diagnosis, pathophysiology and management. *Nat Rev Neurol* 8: 369–379, 2012a. doi:10.1038/nrneurol.2012.97.

Hoeijmakers JG, Han C, Merkies IS, Macala LJ, Lauria G, Gerrits MM, Dib-Hajj SD, Faber CG, Waxman SG. Small nerve fibres, small hands and small feet: a new syndrome of pain, dysautonomia and acromesomelia in a kindred with a novel NaV1.7 mutation. *Brain* 135: 345–358, 2012b. doi:10.1093/brain/awr349.

Imamura H, Nhat KP, Togawa H, Saito K, Iino R, Kato-Yamada Y, Nagai T, Noji H. Visualization of ATP levels inside single living cells with fluorescence resonance energy transfer-based genetically encoded indicators. *Proc Natl Acad Sci USA* 106: 15651–15656, 2009. doi:10.1073/pnas.0904764106.

Izumi Y, Zorumski CF. Neuroprotective effects of pyruvate following NMDA-mediated excitotoxic insults in hippocampal slices. *Neurosci Lett* 478: 131–135, 2010. doi:10.1016/j.neulet.2010.04.078.

Kiernan MC, Bostock H. Effects of membrane polarization and ischaemia on the excitability properties of human motor axons. *Brain* 123: 2542–2551, 2000. doi:10.1093/brain/123.12.2542.

Kitay BM, McCormack R, Wang Y, Tsoulfas P, Zhai RG. Mislocalization of neuronal mitochondria reveals regulation of Wallerian degeneration and NMNAT/WLD(S)-mediated axon protection independent of axonal mitochondria. *Hum Mol Genet* 22: 1601–1614, 2013. doi:10.1093/hmg/ddt009.

Kitayama H, Miura Y, Ando Y, Hoshino S, Ishizaka Y, Koyanagi Y. Human immunodeficiency virus type 1 Vpr inhibits axonal outgrowth through induction of mitochondrial dysfunction. *J Virol* 82: 2528–2542, 2008. doi:10.1128/JVI.02094-07.

Kokotis P, Schmelz M, Kostouros E, Karandreas N, Dimopoulos MA. Oxaliplatin-induced neuropathy: a long-term clinical and neurophysiologic follow-up study. *Clin Colorectal Cancer* 15: e133–e140, 2016. doi:10.1016/j.clcc.2016.02.009.

Lacomis D. Small-fiber neuropathy. *Muscle Nerve* 26: 173–188, 2002. doi:10.1002/mus.10181.

Lark DS, Torres MJ, Lin CT, Ryan TE, Anderson EJ, Neufer PD. Direct real-time quantification of mitochondrial oxidative phosphorylation efficiency in permeabilized skeletal muscle myofibers. *Am J Physiol Cell Physiol* 311: C239–C245, 2016. doi:10.1152/ajpcell.00124.2016.

Lauria G, Cazzato D, Porretta-Serapiglia C, Casanova-Molla J, Taiana M, Penza P, Lombardi R, Faber CG, Merkies IS. Morphometry of dermal nerve fibers in human skin. *Neurology* 77: 242–249, 2011. doi:10.1212/WNL.0b013e318225ab51.

Lehmann HC, Chen W, Borzan J, Mankowski JL, Höke A. Mitochondrial dysfunction in distal axons contributes to human immunodeficiency virus sensory neuropathy. *Ann Neurol* 69: 100–110, 2011. doi:10.1002/ana.22150.

Lenhard W, Lenhard A. *Calculation of Effect Sizes*. Dettelbach, Germany: Psychometrica, 2016. https://www.psychometrica.de/effect_size.html.

Marunaka Y. Effects of internal Na and external K concentrations on Na/K coupling of Na,K-pump in frog skeletal muscle. *J Membr Biol* 101: 19–31, 1988. doi:10.1007/BF01872816.

Nasu S, Misawa S, Nakaseko C, Shibuya K, Isose S, Sekiguchi Y, Mitsuma S, Ohmori S, Iwai Y, Beppu M, Shimizu N, Ohwada C, Takeda Y, Fujimaki Y, Kuwabara S. Bortezomib-induced neuropathy: axonal membrane depolarization precedes development of neuropathy. *Clin Neurophysiol* 125: 381–387, 2014. doi:10.1016/j.clinph.2013.07.014.

Natera-Naranjo O, Kar AN, Aschrafi A, Gervasi NM, Macgibeny MA, Gioio AE, Kaplan BB. Local translation of ATP synthase subunit 9 mRNA alters ATP levels and the production of ROS in the axon. *Mol Cell Neurosci* 49: 263–270, 2012. doi:10.1016/j.mcn.2011.12.006.

Palmgren MG, Nissen P. P-type ATPases. *Annu Rev Biophys* 40: 243–266, 2011. doi:10.1146/annurev.biophys.093008.131331.

Pathak D, Shields LY, Mendelsohn BA, Haddad D, Lin W, Gerencser AA, Kim H, Brand MD, Edwards RH, Nakamura K. The role of mitochondrially derived ATP in synaptic vesicle recycling. *J Biol Chem* 290: 22325–22336, 2015. doi:10.1074/jbc.M115.656405.

Peeling J, Sutherland G, Brown RA, Curry S. Protective effect of dichloroacetate in a rat model of forebrain ischemia. *Neurosci Lett* 208: 21–24, 1996. doi:10.1016/0304-3940(96)12542-8.

Downloaded from journals.physiology.org/journal/jn at Biblioteca Polo Didattico (159.149.193.179) on February 19, 2020.

Pellerin L, Pellegri G, Bittar PG, Charnay Y, Bouras C, Martin JL, Stella N, Magistretti PJ. Evidence supporting the existence of an activity-dependent astrocyte-neuron lactate shuttle. *Dev Neurosci* 20: 291–299, 1998. doi:10.1159/000017324.

Persson AK, Black JA, Gasser A, Cheng X, Fischer TZ, Waxman SG. Sodium-calcium exchanger and multiple sodium channel isoforms in intraepidermal nerve terminals. *Mol Pain* 6: 84, 2010. doi:10.1186/1744-8069-6-84.

Persson AK, Hoeijmakers JG, Estacion M, Black JA, Waxman SG. Sodium channels, mitochondria, and axonal degeneration in peripheral neuropathy. *Trends Mol Med* 22: 377–390, 2016. doi:10.1016/j.molmed.2016.03.008.

Persson AK, Kim I, Zhao P, Estacion M, Black JA, Waxman SG. Sodium channels contribute to degeneration of dorsal root ganglion neurites induced by mitochondrial dysfunction in an in vitro model of axonal injury. *J Neurosci* 33: 19250–19261, 2013a. doi:10.1523/JNEUROSCI.2148-13.2013.

Persson AK, Liu S, Faber CG, Merkies IS, Black JA, Waxman SG. Neuropathy-associated Nav1.7 variant I228M impairs integrity of dorsal root ganglion neuron axons. *Ann Neurol* 73: 140–145, 2013b. doi:10.1002/ana.23725.

Polydefkis M, Yiannoutsos CT, Cohen BA, Hollander H, Schifitto G, Clifford DB, Simpson DM, Katzenstein D, Shriver S, Hauer P, Brown A, Haidich AB, Moo L, McArthur JC. Reduced intraepidermal nerve fiber density in HIV-associated sensory neuropathy. *Neurology* 58: 115–119, 2002. doi:10.1212/WNL.58.1.115.

Press C, Milbrandt J. Nmnat delays axonal degeneration caused by mitochondrial and oxidative stress. *J Neurosci* 28: 4861–4871, 2008. doi:10.1523/JNEUROSCI.0525-08.2008.

Rolyan H, Liu S, Hoeijmakers JG, Faber CG, Merkies IS, Lauria G, Black JA, Waxman SG. A painful neuropathy-associated Nav1.7 mutant leads to time-dependent degeneration of small-diameter axons associated with intracellular Ca^{2+} dysregulation and decrease in ATP levels. *Mol Pain* 12: 1744806916674472, 2016. doi:10.1177/1744806916674472.

Rossignol R, Gilkerson R, Aggeler R, Yamagata K, Remington SJ, Capaldi RA. Energy substrate modulates mitochondrial structure and oxidative capacity in cancer cells. *Cancer Res* 64: 985–993, 2004. doi:10.1158/0008-5472.CAN-03-1101.

Rueda CB, Llorente-Folch I, Amigo I, Contreras L, González-Sánchez P, Martínez-Valero P, Juaristi I, Pardo B, del Arco A, Satrústegui J. Ca^{2+} regulation of mitochondrial function in neurons. *Biochim Biophys Acta* 1837: 1617–1624, 2014. doi:10.1016/j.bbabio.2014.04.010.

Smith AG, Ramachandran P, Tripp S, Singleton JR. Epidermal nerve innervation in impaired glucose tolerance and diabetes-associated neuropathy. *Neurology* 57: 1701–1704, 2001. doi:10.1212/WNL.57.9.1701.

So PW, Fuller BJ. Enhanced energy metabolism during cold hypoxic organ preservation: studies on rat liver after pyruvate supplementation. *Cryobiology* 46: 295–300, 2003. doi:10.1016/S0011-2240(03)00047-6.

Sokoloff L. Energetics of functional activation in neural tissues. *Neurochem Res* 24: 321–329, 1999. doi:10.1023/A:1022534709672.

Takeuchi H, Mizuno T, Zhang G, Wang J, Kawanokuchi J, Kuno R, Suzumura A. Neuritic beading induced by activated microglia is an early feature of neuronal dysfunction toward neuronal death by inhibition of mitochondrial respiration and axonal transport. *J Biol Chem* 280: 10444–10454, 2005. doi:10.1074/jbc.M413863200.

Tanaka T, Nagashima K, Inagaki N, Kioka H, Takashima S, Fukuoka H, Noji H, Kakizuka A, Imamura H. Glucose-stimulated single pancreatic islets sustain increased cytosolic ATP levels during initial Ca^{2+} influx and subsequent Ca^{2+} oscillations. *J Biol Chem* 289: 2205–2216, 2014. doi:10.1074/jbc.M113.499111.

Tanaka Y, Yano H, Ogasawara S, Yoshioka S, Imamura H, Okamoto K, Tsuneoka M. Mild glucose starvation induces KDM2A-mediated H3K36me2 demethylation through AMPK to reduce rRNA transcription and cell proliferation. *Mol Cell Biol* 35: 4170–4184, 2015. doi:10.1128/MCB.00579-15.

Tantama M, Martínez-François JR, Mongeon R, Yellen G. Imaging energy status in live cells with a fluorescent biosensor of the intracellular ATP-to-ADP ratio. *Nat Commun* 4: 2550, 2013. doi:10.1038/ncomms3550.

Verzé L, Paraninfo A, Ramieri G, Viglietti-Panzica C, Panzica GC. Immunocytochemical evidence of plasticity in the nervous structures of the rat lower lip. *Cell Tissue Res* 297: 203–211, 1999. doi:10.1007/s004410051348.

Wang P, Chen M, Yang Z, Yu T, Zhu J, Zhou L, Lin J, Fang X, Huang Z, Jiang L, Tang W. Activation of pyruvate dehydrogenase activity by dichloroacetate improves survival and neurologic outcomes after cardiac arrest in rats. *Shock* 49: 704–711, 2018. doi:10.1097/SHK.0000000000000971.

Wendt HW. Dealing with a common problem in social science: a simplified rank-biserial coefficient of correlation based on the *U* statistic. *Eur J Soc Psychol* 2: 463–465, 1972. doi:10.1002/ejsp.2420020412.

Westermann B. Bioenergetic role of mitochondrial fusion and fission. *Biochim Biophys Acta* 1817: 1833–1838, 2012. doi:10.1016/j.bbabio.2012.02.033.

Youle RJ, van der Bliek AM. Mitochondrial fission, fusion, and stress. *Science* 337: 1062–1065, 2012. doi:10.1126/science.1219855.

Zeng J, Yang GY, Ying W, Kelly M, Hirai K, James TL, Swanson RA, Litt L. Pyruvate improves recovery after PARP-1-associated energy failure induced by oxidative stress in neonatal rat cerebrocortical slices. *J Cereb Blood Flow Metab* 27: 304–315, 2007. doi:10.1038/sj.jcbfm.9600335.

Downloaded from journals.physiology.org/journal/jn at Biblioteca Polo Didattico (159.149.193.179) on February 19, 2020.